

Averaged Euler Equations, Vortex Blobs, and Second Grade Fluids

By **BALU T. NADIGA**¹, AND **STEVE SHKOLLER**² †

¹Earth and Environmental Sciences, MS-B296, Los Alamos NM 87545 USA
email:balu@lanl.gov

²Department of Mathematics, University of California, Davis CA 95616 USA
email:shkoller@math.ucdavis.edu

Add new abstract.

1. Introduction

The two-dimensional Euler equations for a perfect incompressible fluid are given by

$$\begin{aligned} \partial_t \omega(t, x) + \operatorname{div}[\omega(t, x) \cdot u(t, x)] &= 0, \\ \operatorname{div} u &= 0, \quad \omega = \operatorname{curl} u, \\ \omega(0, x) &= \omega_0(x), \end{aligned} \tag{1.1}$$

where $\omega(t, x)$ is the vorticity function, $u(t, x)$ is the spatial velocity vector field, t denotes time, and $x = (x_1, x_2)$ denotes the Cartesian coordinates in the plane. Inverting the vorticity-velocity relation, we have that

$$u(t, x) = \int \int K(x, y) \omega(t, y) dy, \tag{1.2}$$

where $K = \nabla^\perp G$ and G is the solution of $-\Delta G = \delta$ and $\nabla^\perp = (-\partial_{x_1}, \partial_{x_2})$. For fluid motion over the entire plane, $K(x, y) = (2\pi)^{-1} \nabla^\perp \log|x - y|$. Let $\eta_t(x) = \eta(t, x)$ denote the flow of u so that

$$\partial_t \eta(t, x) = u(t, \eta(t, x)). \tag{1.3}$$

Because u is divergence-free, the flow map η_t is an area-preserving transformation. It follows that

$$\begin{aligned} \partial_t \eta(t, x) &= \int \int K(\eta_t(x), \eta_t(y)) \omega(t, \eta_t(y)) dy \\ &= \int \int K(\eta_t(x), \eta_t(y)) \omega_0(y) dy \end{aligned} \tag{1.4}$$

(1.5)

where the last equality follows from the pointwise conservation of vorticity along Lagrangian trajectories, $\omega(t, \eta_t(x)) = \omega_0(x)$. Hence, it is clear that the initial vorticity field completely determines the fluid motion. When the initial vorticity is a sum of N point vortices δ_i positioned at the points x_i in the plane with circulations Γ_i , i.e., $\omega_0 = \sum_{i=1}^N \Gamma_i \delta_i$, then (1.4) gives the classical point-vortex approximation to (1.1), but as a numerical

† Present address: Center for Nonlinear Studies, Los Alamos National Laboratory, MS-B258, Los Alamos NM 87545

method for approximating the Euler flow with arbitrary initial vorticity functions, the method is known to be unstable.

Chorin's vortex blob method alleviates the instability of the point-vortex scheme by smoothing each delta function δ_i with a vortex blob χ^α , a function that decays at infinity, and whose mass is mostly supported in a disc of diameter α . Thus, instead of using the integral kernel $K(x, y)$, one instead uses the smoother kernel $K^\alpha = \nabla^\perp G^\alpha$ where G^α is the solution of

$$-\Delta G^\alpha = \chi^\alpha.$$

The vortex-blob method then evolves the point-vortex initial data, which we shall now call q_0 , by the ordinary differential equation

$$\partial_t \eta(t, x) = \int \int K^\alpha(\eta_t^\alpha(x), \eta_t^\alpha(y)) q_0(y) dy. \quad (1.6)$$

Hald has shown that when K^α is a Bessel function or a polynomial of Bessel functions, the vortex method has infinite-order accuracy. When the vortex-blob K^α is a modified Bessel function of the second kind, it is the fundamental solution of the operator $(1 - \alpha^2 \Delta)$ in the plane, so that if $u^\alpha(t, x) = \int \int K^\alpha(x, y) q(y) dy$, then the vorticity q is related to the smoothed velocity vector field u^α by $q = (1 - \alpha^2 \Delta) \text{curl } u^\alpha$. Thus, Chorin's vortex method is actually given by the PDE

$$\begin{aligned} \partial_t q(t, x) + \text{div}[q(t, x) \cdot u^\alpha(t, x)] &= 0, \\ \text{div } u &= 0, \quad q = (1 - \alpha^2 \Delta) \text{curl } u^\alpha, \\ q(0, x) &= q_0(x). \end{aligned} \quad (1.7)$$

Remarkably, this PDE is exactly the equation for a second-grade non-Newtonian inviscid fluid, when the constant $\alpha > 0$ is interpreted as a material parameter which measures the elastic response of the fluid due to polymerization. To see this, we may reexpress (1.1) as an evolution equation for the velocity $u^\alpha(t, x)$. Temporarily dropping the superscript α , (1.7) is equivalent to

$$\partial_t (1 - \alpha^2 \Delta) u(t, x) + \text{curl}(1 - \alpha^2 \Delta) u(t, x) \times u(t, x) = -\text{grad } p(t, x), \quad (1.8)$$

which is the traditional form of the second-grade fluid equations Dunn & Fosdick (1974) (of course, one can add viscosity $-\nu \Delta u$ to the left-hand-side). According to Noll's theory of simple materials, (1.8) is governed by the unique constitutive law that satisfies material frame-indifference and observed objectivity. Consequently, the vortex method with the Bessel function smoothing naturally inherits these important characteristics. In light of the fact that some authors have stated that turbulence is like polymer flow, we find this connection between a classical numerical algorithm and a well established constitutive theory for polymeric flow to be quite intriguing.

In addition to this surprising connection, there is also a beautiful geometric structure to the vortex method which follows the framework developed by Arnold (1966) and Ebin & Marsden (1970). While the details of this particular issue are far outside the scope of this article, it is, nevertheless, worthwhile to state the result. Arnold showed that the appropriate configuration space for a perfect incompressible fluid is the group of all area preserving diffeomorphisms of the fluid container, and that solutions of the Euler equations are geodesics on this group with respect to a certain kinetic energy metric, characterized by the inner-product $\int \int u(x) \cdot v(x) dx$ for two vector fields u and v . The vortex blob method also has this geometric property, but now the metric is instead

characterized by

$$\int \int [u(x) \cdot v(x) + 2\alpha^2 \text{Def } u(x) \cdot \text{Def } v(x)] dx,$$

where $\text{Def } u$ is the rate of deformation tensor (see Shkoller (1999) for the geometry and analysis of the vortex dynamics).

The vortex method numerical scheme thus preserves the Hamiltonian structure of the Euler equations. In particular, vorticity remains pointwise conserved by the smooth Lagrangian flow η_t^α so that

$$q(t, \eta_t^\alpha(x)) = q_0(x),$$

the vorticity momenta

$$I_p = \int \int q^p dx$$

are conserved, and so the Kelvin circulation theorem remains intact as well.

Because we have the PDE (1.7) that governs the vortex method, we can now consider the spectral truncation of (1.7) for an arbitrary initial vorticity function q_0 , and study the vortex dynamics of such a numerical approximation, and in particular, compare the vortex-blob dynamics to the spectrally-truncated Euler dynamics. In order to obtain numerically resolved simulations, we use biharmonic dissipation with the minimal viscosity ν for which resolution is attained. Based on our numerical experiments, we find that for the above fixed value of ν , the vortex method ($\alpha > 0$)

1. cuts-off the energy spectrum at small scales faster than for the dissipative Euler equations, while leaving the large scale spectrum essentially unchanged;
2. produces significantly smaller decay of the kinetic energy than the Euler equations (using the same dissipation and numerical resolution);
3. leaves the entire enstrophy spectrum essentially unchanged, preserving the fundamental sharp decay of enstrophy during the vortex merger process.

Although the addition of viscosity is essential for obtaining numerical resolution (and hence meaningful results), it is interesting to compare the inviscid dynamics of the spectral truncations of the vortex method and the Euler equations when $\nu = 0$. We find that the vortex method for $\alpha > 0$ provides a dispersive regularization of the conservative Euler dynamics, and while preserving the correct large scale dynamics, the scheme is able to filter the small scale noise in Euler which is traditionally removed by the addition of viscous dissipation.

While our focus has thus far been relegated to the effect of vortex-blob smoothing of traditional Euler dynamics, our computational studies also reflect the dynamical attributes of polymerization of a Newtonian fluid, and in particular, the role of slight (for small α) elasticity of the fluid. Restating our observations in this non-Newtonian framework, we find that a small amount of polymerization has the effect of smoothing small scale motion, cutting-off the slope of the energy spectrum, and maintaining (even quantitatively) the large scale features of the flow.

2. Numerical Simulations

In this section, we will consider both forced-dissipative and unforced-inviscid simulations of the Euler and Euler- α equations to demonstrate the effect of the inviscid modification to the advective nonlinearity of the Euler equations.

2.1. Formulation

The evolution of both the Euler and Euler- α systems we consider in this article is governed by

$$\frac{\partial \omega}{\partial t} + (1 - \alpha^2 \nabla^2)^{-1} J[\psi, (1 - \alpha^2 \nabla^2) \omega] = F + D; \quad \nabla^2 \psi = \omega, \quad (2.1)$$

where a vorticity-stream function formulation is used and all notation is as previously defined. In the above equations, the Euler system corresponds to $\alpha = 0$.

For simplicity we work on a doubly periodic domain of length 2π on a side and work with Fourier modes. Considering Fourier modes with wavenumbers in the set \mathbf{k} given by

$$\mathbf{k} \equiv \{k = (k_x, k_y), \quad 0 \leq k_x, k_y \leq k_{max}, \quad k_x, k_y \text{ integers}\}, \quad (2.2)$$

the Galerkin projection of (2.1) on to these modes results in

$$\frac{d}{dt} \hat{\omega}_k + \frac{1}{1 + (|k|/k_\alpha)^2} \sum_{\substack{m+n=k \\ k, m, n \in \mathbf{k}}} (1 + (|n|/k_\alpha)^2) \frac{m \times n}{|m|^2} \hat{\omega}_m \hat{\omega}_n = \hat{F} + \hat{D}, \quad (2.3)$$

where $\hat{\omega}$ is the Fourier transform of ω and k_α is the wavenumber corresponding to α . Under such a truncation, among the infinity of inviscid ($F = D = 0$) conserved quantities for (2.1), the only two conservation properties that survive are those for the kinetic energy E_{H^1} , given by

$$E_{H^1} = \frac{1}{2} \int_M (|u|^2 + \alpha^2 |\nabla u|^2) d\mathbf{x} \quad (= \|u\|_{H^1}^2). \quad (2.4)$$

and enstrophy Z_{H^2} given by

$$Z_{H^2} = \frac{1}{2} \int_M [(1 - \alpha^2 \nabla^2) \omega]^2 d\mathbf{x} \quad (= \|\omega\|_{H^2}^2). \quad (2.5)$$

Although the inviscid conserved energy is E_{H^1} and the inviscid conserved enstrophy is Z_{H^2} , we will concern ourselves with the dynamics of the usual kinetic energy and usual enstrophy as given by

$$E = \frac{1}{2} \int_M |u|^2 d\mathbf{x}, \quad (2.6)$$

$$Z = \frac{1}{2} \int_M \omega^2 d\mathbf{x}. \quad (2.7)$$

This is because, our intent in this article is to use the Euler system as the reference and then to consider the modifications due to nonzero α in (2.1). Only the usual energy and enstrophy as defined in (2.6) and (2.7) are relevant in the reference Euler system.

Equation (2.3) is implemented numerically using a fully dealiased pseudospectra method (see Canuto (1988)), in which the dealiasing is achieved using the two-thirds rule (also called the three-halves rule) wherein only two-thirds of the Fourier modes are used and the highest wavenumber-third of the Fourier modes are zero-padded. (This is equivalent to computing the nonlinear terms in physical space at three-halves the number of points as the number of Fourier modes used.) Conservations (2.4) and (2.5) are thus respected exactly by the spatial discretization.

We remark that we repeated some of the computations using the Arakawa second-order finite difference spatial discretization. This scheme also respects the conservations (2.4) and (2.5) and uses the Arakawa Jacobian, $J_A[\psi, \omega]$, for $J[\psi, \omega]$, and where $J_A[\psi, \omega]$ is

given by

$$J_A[\psi, \omega] = \frac{1}{3} \left(\psi_y \omega_x - \psi_x \omega_y + (\psi_y \omega)_x - (\psi_x \omega)_y + (\psi \omega_x)_y - (\psi \omega_y)_x \right), \quad (2.8)$$

(see Arakawa (1966)). In the above equation, each of the partial derivative is replaced by its central difference quotient. The numerical results this scheme produced were qualitatively identical to those produced by the spectral method.

As for the temporal discretization, we use a (nominally) fifth-order, adaptive timestep, embedded Runge-Kutta Cash-Karp algorithm (see Press et al. (1992)). This scheme is advantageous over the more traditional leapfrog timestepping as it does not have a spurious computational mode and it allows for variable timestepping to be implemented in a straightforward manner. One step of this method uses six functional evaluations at appropriate points which are combined in two different ways to produce a fourth-order and a fifth-order increment, thereby allowing an estimate of the fifth-order error. This method of adaptive timestepping is approximately twice as efficient as Runge-Kutta methods based on timestep doubling. By requiring

$$\frac{\max |E_5(\omega_k, \omega_{k+1})|}{\max |\omega_k|} < 10^{-7},$$

energy error was (on average) less than one hundredth of a percent (0.01%) and enstrophy error was less than one tenth of one percent (0.10%) during the course of the inviscid simulations that we performed.

We choose initial conditions so that the initial energy spectrum scales as

$$E(k) \sim k \exp\left(-\frac{k}{k_0}\right), \quad (2.9)$$

where k_0 is chosen to be 2. Further, the amplitude for each mode is drawn from a zero-mean normal distribution of random numbers. For convenience, we measure time in terms of the initial large eddy turnover time, τ , which is defined as

$$\tau = \frac{2\pi k_i^{-1}}{u'}.$$

Here, k_i represents the integral scale of the initial condition, found as a ratio of its enstrophy to energy:

$$k_i = \sqrt{\frac{Z}{E}} \quad (2.10)$$

and the mean fluctuation velocity u' is calculated as

$$u' = \sqrt{2E}$$

Henceforth, if the unit of time is not mentioned, it should be assumed to be in terms of the initial large eddy turnover time.

2.2. Forced-Dissipative Cases

In the forced-dissipative runs to be considered in this section, the forcing F is achieved by keeping the amplitudes of modes with wavenumbers in the small wavenumber band $10 \leq k < 10.001$ constant in time. The dissipation, D , is a combination of a fourth order hyperviscous operator and a large-scale friction term:

$$D = \delta\psi - (-\nu\nabla^2)^4 \omega.$$

As has been used in numerous previous studies of two-dimensional turbulence (e.g., see ?), we use this form of the dissipation operator in order to satisfy the difficult requirements of having to resolve the flow and at the same time reach a statistically steady state in a fairly inviscid regime and with reasonably small computational resources in this preliminary study. The form and value of the forcing and dissipation are held exactly the same for all the runs to be presented, irrespective of the resolution and the value of α . For reference, we show in Fig. 2.1, the vorticity field for the case $\alpha = 0$ at time 20, when the system has reached statistically stationarity.

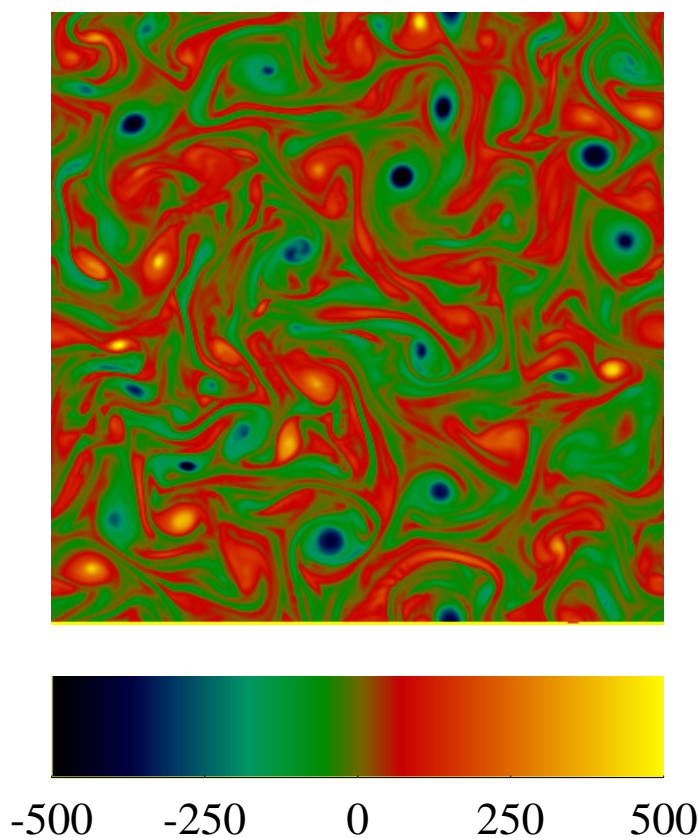


FIGURE 2.1. Vorticity field when the system has reached statistically stationarity.

Fig. 2.2 shows the evolution of the kinetic energy E with time for four different values of k_α . For these computations, 256 physical grid points were used in each direction, resulting in, after accounting for dealiasing, a maximum, circularly-symmetric wavenumber, k_{max} (see 2.2) of 85. The four runs correspond to k_α of ∞ (dissipative Euler) and 42, 21, and 7. We remind the reader, that but for the difference in the values of k_α , the four runs are identical. This figure shows that for identical forcing and dissipation, the tendency with increasing α (equivalently decreasing k_α) is to achieve an overall balance which makes

the flow less viscous. To further examine the nature of this reduced-viscous behavior, we examine the energy-wavenumber spectra for these four cases in Fig. 2.2. Here, the average of the one dimensional energy spectrum $E(k)$ between times 5 and 20 is plotted against the scalar wavenumber k . Figure 2.2 shows that the reduced-viscous behavior for increasing α is achieved by systematically increasing the energy in modes larger in scale than the forcing scale and decreasing the energy in modes smaller in scale compared to the forcing scale. The larger energy content in the larger scales (smaller wavenumbers) is a reflection of the enhancement of the inverse cascade of energy of two-dimensional turbulence by the nonlinear-dispersive modification of the advective nonlinearity when $\alpha > 0$ in (2.1). So also, the decreased energy content in the smaller scales (larger wavenumbers) is attributable to the same nonlinear-dispersive modification and is a reflection of the fact that at these scales, the enstrophy that is cascading is not the usual enstrophy as defined in (2.7), but actually the enstrophy as defined in (2.5) (and which would be conserved in an inviscid and unforced case). The overall effect of increased inverse energy cascade and depressed energy levels in the high modes are shown in Fig. 2.4, where the time-evolution of the integral wavenumber scale k_i , as defined in (2.10), is shown for the same four cases: with decreasing k_α , k_i is also decreasing.

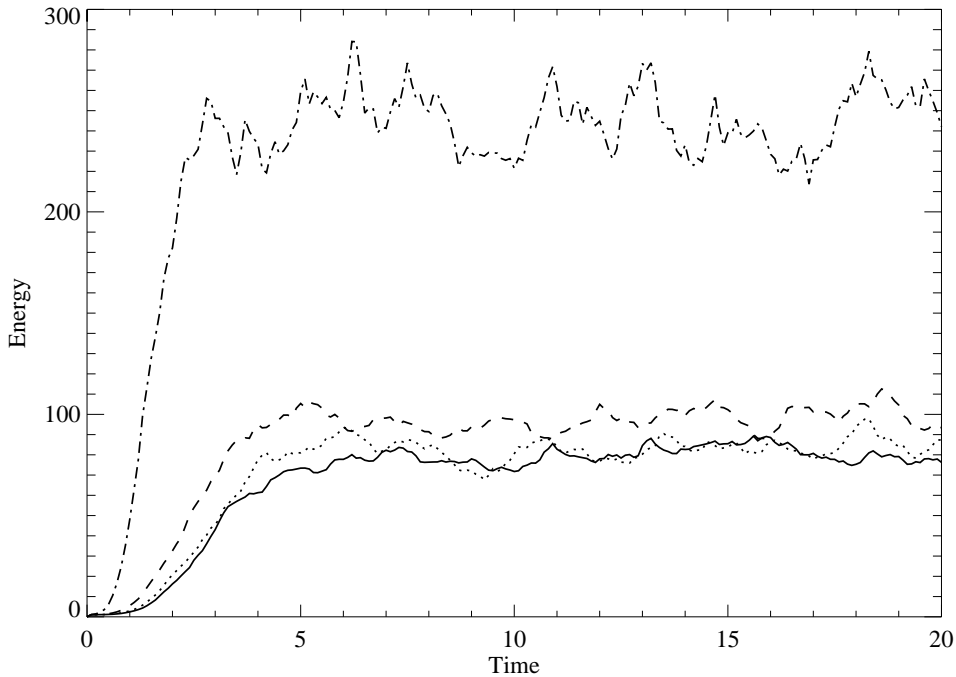
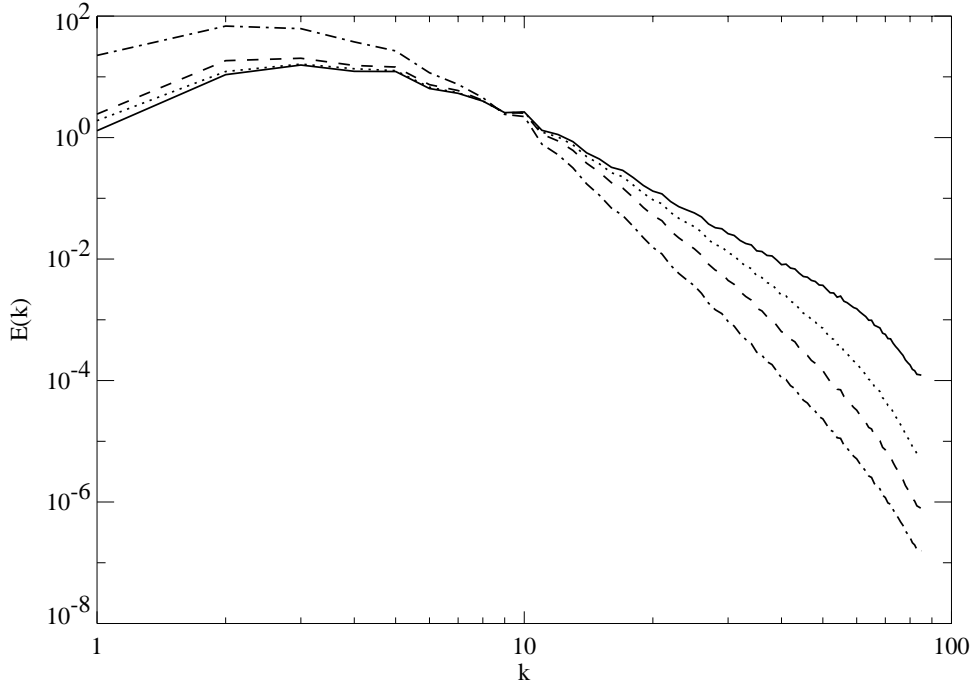


FIGURE 2.2. Kinetic energy vs. time

We can carry out a Kolmogorov-like dimensional argument to estimate the scaling of the energy spectrum in the enstrophy cascade inertial regime, if we assume that the wavenumber k_α only appears in the Helmholtz operator. Thus, in this regime,

$$E(k) \sim \beta_{H^2}^a k^b, \quad (2.11)$$

where β_{H^2} is the rate of dissipation of Z_{H^2} enstrophy, and a and b are exponents to be


 FIGURE 2.3. $k_\alpha = \infty, 42, 21,$ and 7 .

stationarity.

determined by dimensional analysis. A dimensional analysis of (2.11), leads to

$$L^3 T^{-2} = T^{-3a} L^{-b} (1 + \alpha^2 L^{-2})^{2a},$$

from which $a = 2/3$. However, even in the enstrophy cascade regime, the value of b depends on the ratio α/L . For $\alpha \ll L$, of course, $b = -3$, or the classical $E(k)^{-3}$ is recovered. So, also when $\alpha \gg L$, $E(k) \sim k^{-\frac{17}{3}}$. Finally, when α is comparable to L , it is easy to see that $E(k)$ falls off faster than the corresponding fall-off for Euler (verified in Fig. 2.2, but slower than $k^{-\frac{17}{3}}$). We defer the verification of the exact values of the exponent b to later studies when we can afford much larger simulations with a good dynamic range in the inertial regime.

The steeper fall-off the energy spectrum with k in the enstrophy cascade range of wavenumbers when $\alpha > 0$, compared to Euler may, at first, suggest that a coarser resolution may be sufficient to resolve the flow when $\alpha > 0$ (for the same forcing and dissipation). However, this is not the case, as should be clear from Fig. 2.2. In this figure, the spectra of the four cases previously discussed is replotted using solid lines, and the spectra drawn using dashed lines are from four new runs where everything is held exactly the same, but the resolution is reduced in half ($k_{max} = 42$). The degree of non-resolution of the flow with this reduced resolution is indicated by the degree of deviation of the dashed-line spectrum from the solid-line spectrum, and this seems to be independent of α to the leading order.

2.3. Unforced-Inviscid Cases

The finiteness of resolution is not a problem when the flow is fully resolved by the a priori fixed resolution as in the first four computations of the previous section. On the other

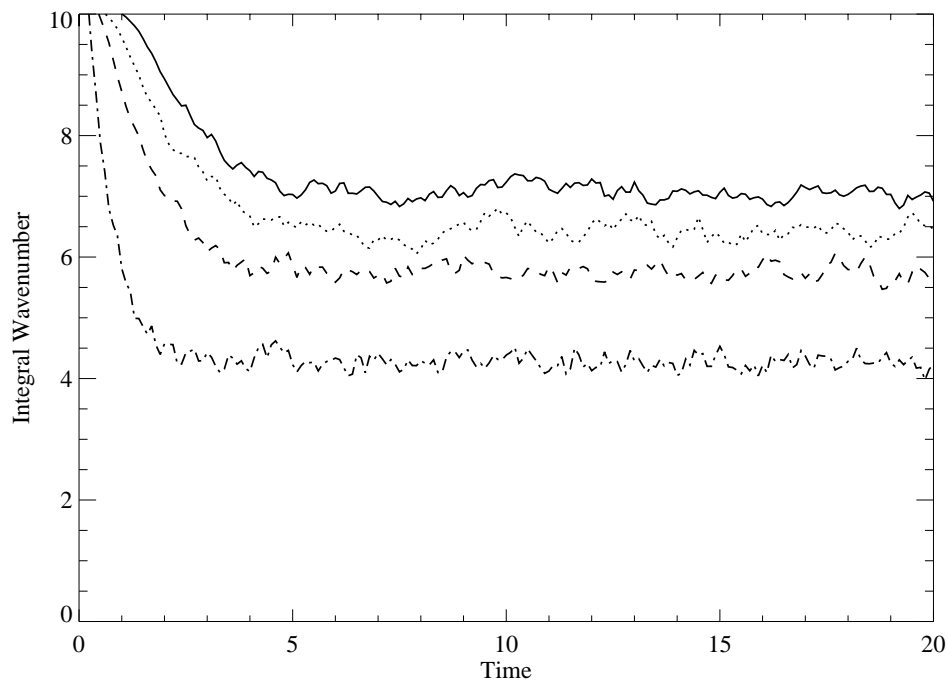


FIGURE 2.4. Integral wavenumber vs. time

hand an inviscid system, either Euler or Euler- α will outrun any given resolution, however high; when this will happen is a question of the initial conditions, the value of α and the chosen resolution. But we think there is use to considering the *finite* truncation (2.3) even when ν_4 is identically zero, and the flow is, by definition, poorly resolved. This is not to suggest that such computations are directly physically relevant, but only that one may learn aspects of the system which are chosen to model the original physical situation. Sometimes, this may in turn be useful in checking the consistency or a lack of it with respect to certain hypothesized processes in the original system. It is in this spirit that we now go on to consider the long time states of the inviscid Euler and Euler- α systems truncated to be closed under our a priori fixed resolution.

The setup for the new simulations we present now are identical to those for the previous simulations, but with F and D identically zero in each of the cases. In the initial few characteristic times, there is a downscale cascade of enstrophy and an upscale cascade of energy from the given initial conditions resulting in the system encountering the finite bounds imposed by the truncation. Thereafter, the solutions of the truncated system are not representative of the solutions of the untruncated system and the nonlinearity acts to thermalize the system while respecting the dual conservation of kinetic energy and enstrophy ((2.4 and (2.5)). This results in statistical equilibria of the kind considered in Kraichnan & Montgomery (1967) (and references therein) for $\alpha = 0$ and Nadiga (1999) for $\alpha \neq 0$. We also note that conservation requirements impose rather strict numerical time step requirements in the inviscid cases.

The initial conditions previous described are so as to correspond to negative temperature states from the statistical mechanical point of view (see Kraichnan & Montgomery (1967) and references therein and Nadiga (1999)), simply meaning that the lowest modes

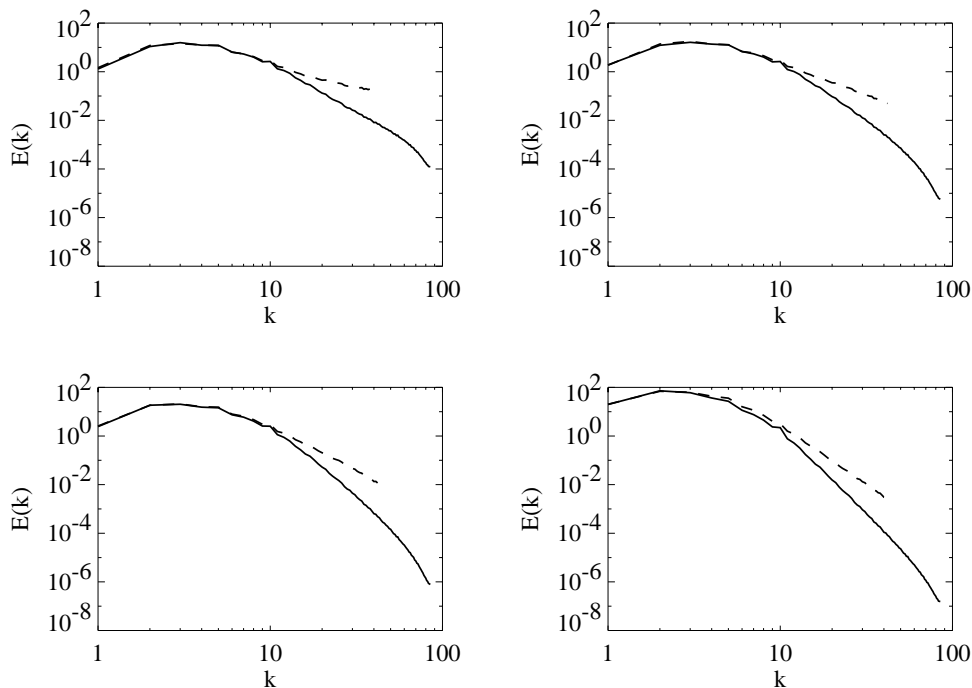


FIGURE 2.5. Halved resolution

stationarity.

of the system are excited to high enough amplitudes to give rise to coherent looking physical structures, but with a nontrivial distribution of energy in the higher modes. In fact, the spectra in Fig. 2.6 compare the excitation of the various modes at different values of α . These spectra are averaged in time between 45 and 60 to average over statistical fluctuations after the systems have settled in their respective statistical equilibria. Clearly, the most significant differences occur at large wavenumbers with the energy at high wavenumbers getting smaller with increasing α . Actually, for $\alpha \neq 0$, a two-constraint statistical theory anticipates a more rapid decay of the one-dimensional energy spectrum:

$$E(k) \sim k^{-5},$$

as compared to

$$E(k) \sim k^{-1},$$

for $\alpha = 0$ (see Nadiga (1999) for details), and this is clearly verified in Fig. 2.6.

3. Concluding Remarks

Acknowledgments

The authors thank Jerry Marsden, and David Montgomery for extensive discussions on a variety of issues related to this article. BTN was supported by the Climate Change Prediction Program of the Department of Energy and SS was partially supported by NSF-KDI grant ATM-98-73133.

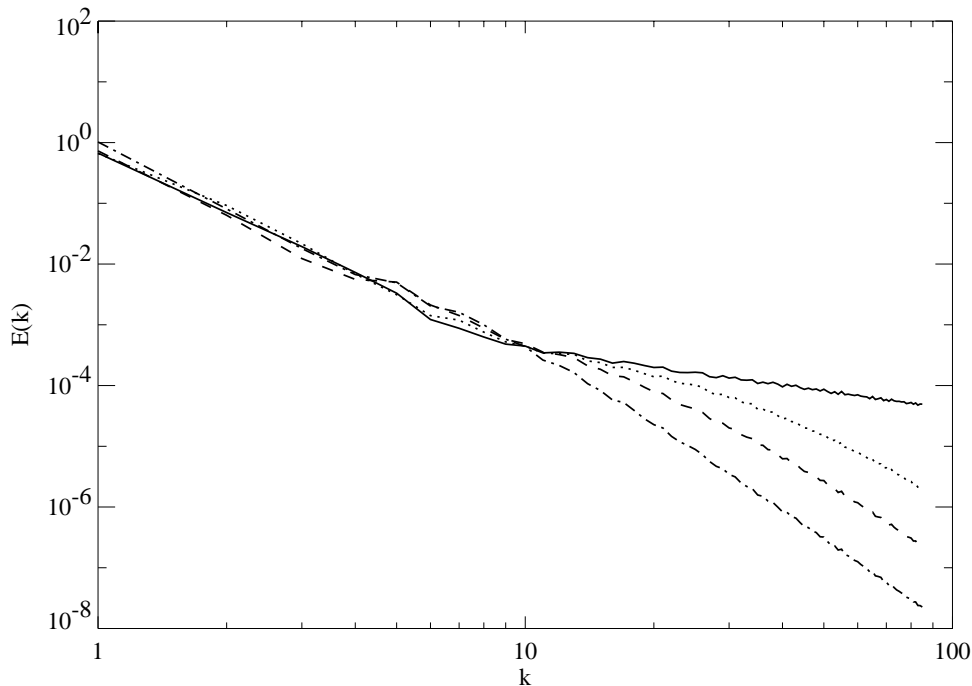


FIGURE 2.6. Unforced-inviscid. Statistical equilibration

- A. ARAKAWA, *Computational design for long-term numerical integration of the equations of fluid motion: Two-dimensional incompressible flow, Part 1*, J. Comput. Phys., **1**, (1966), 119-143.
- V.I. ARNOLD, *Sur la geometrie differentielle des groupes de Lie de dimension infinie et ses applications a l'hydrodynamique des fluids parfaits*, Ann. Inst. Grenoble, **16**, (1966), 319-361.
- G.I. BARENBLATT AND A.J. CHORIN, *New Perspectives in turbulence: scaling laws, asymptotics, and intermittency*, SIAM Rev., **40**, (1998), 265-291.
- C. BASDEVANT & R. SADOURNY *Ergodic Properties of inviscid truncated models of two-dimensional incompressible flows*, J. Fluid Mech., **69**, (1975), 673-688.
- C. CANUTO, *Spectral methods in fluid dynamics*, Springer-Verlag, New York, 1988.
- S. CHEN, D.D. HOLM, L. MARGOLIN, AND R. ZHANG, *Direct numerical simulations of the Navier-Stokes alpha model*, (1999), preprint.
- J.E. DUNN AND R.L. FOSDICK, *Thermodynamics, stability and boundedness of fluids of complexity 2 and fluids of second grade*, Arch. Rat. Mech. Anal., **56**, (1974), 191-252.
- D. EBIN AND J. MARSDEN, *Groups of diffeomorphisms and the motion of an incompressible fluid*, Ann. of Math., **92**, (1970), 102-163.
- D.G. FOX & S.A. ORSZAG, *Inviscid dynamics of two-dimensional turbulence*, Phys. Fluids, **16**, (1973), 169-171.
- R.H. KRAICHNAN, *Inertial ranges in two-dimensional turbulence*, Phys. Fluids, **10**, (1967), 1417-1423.
- R.H. KRAICHNAN AND D.MONTGOMERY, *Two-dimensional turbulence*, Reports on progress in physics, **43**, (1980), 547-619.
- A. MAJDA AND M. HOLEN, *DISSIPATION, TOPOGRAPHY, AND STATISTICAL THEORIES FOR LARGE-SCALE COHERENT STRUCTURE*, Comm. Pure Appl. Math. **50**, (1997), 1183-1234.
- W.H. MATTHAEUS AND D. MONTGOMERY, *Selective decay hypothesis at high mechanical and magnetic reynolds-numbers*, Annals of the New York academy of sciences, **357**, (1980), 203-222.

- J.C. MCWILLIAMS, *The emergence of isolated vortices in turbulent flow*, J. Fluid Mech., **146**, (1984), 21–34.
- J. MILLER, P.B. WEICHMAN, AND M.C. CROSS, *Statistical-mechanics, Euler equation, and Jupiter's red spot*, Phys. Rev. A, **45**, (1992), 2328–2359.
- B.T. NADIGA, *Scaling properties of an inviscid mean-motion fluid model*, J. Stat. Phys, (to appear)
- B.T. NADIGA AND L.G. MARGOLIN, *Dispersive eddy parameterization in a barotropic ocean model*, in preparation.
- E.A. OVERMAN AND N.J. ZABUSKY, *Evolution and merging of isolated vortex structures*, Phys. Fluids, **25**, (1982), 1297–1305.
- W.H. PRESS, B.P. FLANNERY, S.A. TEUKOLSKY, & W.T. VETTERLING, *Numerical Recipes in Fortran 77*, Cambridge University Press, (1992), 708–716.
- R. ROBERT AND J. SOMMERIA, *Statistical equilibrium states for 2-dimensional flows*, J. Fluid Mech., **229**, (1991), 291–310.
- R. SADOURNY AND C. BASDEVANT, *Parameterization of subgrid scale barotropic and baroclinic eddies in quasi-geostrophic models: Anticipated Potential Vorticity method*, J. Atmos. Sciences, **42**, (1985), 1353–1363.
- S. SHKOLLER, *Groups of diffeomorphisms for manifolds with boundary and hydrodynamics*, (1999), E-print math.AP/9908109.